

Importance of Metastable States in the Free Energy Landscapes of Polypeptide Chains

Stefan Auer,¹ Mark A. Miller,¹ Sergei V. Krivov,² Christopher
M. Dobson,¹ Martin Karplus,^{2,3} and Michele Vendruscolo¹

¹*University Chemical Laboratory, Lensfield Road, Cambridge CB2 1EW, United Kingdom*

²*Laboratoire de Chimie Biophysique, ISIS, Université Louis Pasteur, 67000 Strasbourg, France*

³*Department of Chemistry and Chemical Biology, Harvard University, Cambridge, MA 02138*

(Dated: January 18, 2018)

We show that the interplay between excluded volume effects, hydrophobicity, and hydrogen bonding of a tube-like representation of a polypeptide chain gives rise to free energy landscapes that exhibit a small number of metastable minima corresponding to common structural motifs observed in proteins. The complexity of the landscape increases only moderately with the length of the chain. Analysis of the temperature dependence of these landscapes reveals that the stability of specific metastable states is maximal at a temperature close to the mid-point of folding. These metastable states are therefore likely to be of particular significance in determining the generic tendency of proteins to aggregate into potentially pathogenic agents.

PACS numbers: 87.15.Aa, 87.14.Ee

The mechanism by which proteins fold reliably into their native states is frequently described by using the concept of a free energy landscape (FEL) [1, 2, 3, 4]. Under physiological conditions, the region of configuration space associated with the native state has the lowest free energy and is therefore thermodynamically the most stable. In addition to the native and fully unfolded states, intermediate structures have been detected in the folding and misfolding processes of many proteins [5, 6, 7, 8]. These metastable states can play an important role in the folding process, or be kinetic traps that interfere with correct folding. The experimental characterization of these states remains challenging, as they are often transient or disordered, but significant progress in this direction has recently been made by combining experiment with theory [8, 9, 10]. Since specific metastable states can increase the probability of misfolding and aggregation [11, 12], it is important to understand the mechanism of their formation. Indeed, a global characterization of the FEL is crucial to a full understanding of the relationship between the native and metastable states, and the interplay between folding and misfolding.

A complete characterization of the FEL by computational methods requires that the free energies of the native and all non-native structures be calculated. Two problems arise in this exercise: the technical issue of sampling a vast number of configurations separated by a variety of free energy barriers, and the conceptual difficulty of choosing an appropriate set of coordinates to describe the FEL [13]. Sampling is typically performed in the vicinity of an ensemble of folding or unfolding pathways, and the resulting free energy is then projected on to a subspace defined by one or two order parameters [3]. For the resulting surfaces to provide insight into thermodynamics and dynamics, it is crucial that the chosen order parameters are able to detect the relevant details of the FEL. In cases where a long dynamic trajectory that explores a large region of configuration space is available,

it is possible to mitigate the order parameter problem by using the dynamics to cluster the configurations and disconnectivity graphs to represent the results [14]. To maintain the dynamic approach but improve the extent of sampling, methods have been developed that start from a survey of local minima on the *potential* energy landscape [15]. A related approach has been used in which potential energy minima are grouped together by a dynamic criterion based on an approximate rate theory before their combined free energies are calculated [16].

The level of detail in which a FEL can be computed depends on the choice of protein model. For fully atomistic representations, analysis has been restricted mostly to peptides and small proteins [2, 3]. Coarse-grained descriptions allow larger regions of the conformational space to be explored. In the most tractable models proteins are confined to a lattice [17]. A great deal of valuable insight has been gained from this approach, but there are limits to how realistic it can be made. A promising new model has recently been proposed whose distinctive feature is that the protein backbone is assigned a finite thickness to account in an effective way for the volume occupied by the amino acid side chains [18, 19, 20]. The interactions considered include directional hydrogen bonding (with well depth e_{HB}), a local bending stiffness (defined by an energy penalty e_{S}), and pairwise attractive hydrophobic forces (with energy e_{W}). The protein is thus regarded as a semi-flexible tube whose radial symmetry is broken by the restraints imposed by the hydrogen bonds. The excluded volume of the tube makes this model significantly different from other off-lattice coarse-grained models such as beads-on-strings, and also from $G\ddot{o}$ models because it includes no explicit energetic bias towards a predetermined structure.

The zero-temperature phase diagram of a 24-residue homopolymer was characterised by using this approach as a function of hydrophobic strength and stiffness, each measured relative to the hydrogen bonding strength [18].

The resulting set of ground states, similar to those annotating the figures in this Letter, show a remarkable resemblance to the structures deposited in the protein data bank [21], indicating that the model is capable of capturing the range of folds available to a real polypeptide chain. The directionality of the hydrogen bonding, together with the excluded volume of the tube (or secondary structure requirements, as shown recently in a related model [22]) confine the energetically favorable conformations of a polypeptide chain to a small subset of those that would exist in the absence of such restrictions.

In this Letter, we look beyond the global minima of the potential energy surfaces, and characterize the entire FEL of the tube model at finite temperatures. By repeating the calculations for different values of the parameters we examine the effect of hydrophobicity and stiffness on both native and metastable states. We also determine how the relationship between the various structures on the FEL changes with temperature, which has important implications for understanding the competition between folding, misfolding and aggregation.

Projecting a FEL on to any set of order parameters runs the risk of concealing or distorting features of the folding process. To introduce as little prejudice as possible, we start by plotting a transition disconnectivity graph (TRDG) [14, 15] in which configurations along a continuous ergodic trajectory, generated by crankshaft and pivot Monte Carlo steps, are clustered according to their all-atom root-mean-square displacement (RMSD) using a threshold of 2.2\AA . The trajectory is mapped onto a graph of nodes, each representing a cluster of configurations, and edges weighted by the number of transitions between pairs of clusters. The partition function Z of a cluster is proportional to its residence time in the simulation, while that of a transition state between any pair of nodes is given by the minimum cut that separates them on the graph [14, 15]. In both cases, the partition function is related to the free energy by $F/kT = -\ln Z$. The TRDG is constructed from these free energies by placing nodes on a vertical free energy scale and connecting them at a point according to the free energy of the transition state that connects them.

For stiffness $e_S = 0.4$ and hydrophobicity $e_W = 0.05$ at temperature $T^* = 0.161$ (where all quantities are specified in units of e_{HB}), a simulation was run for a sufficiently long time to observe spontaneous folding and unfolding about 100 times. The resulting TRDG is shown in Fig. 1(a). Most of the branches from the main stem are vertically short, indicating low barriers and thus a smooth surface. The main feature is a well-defined stem corresponding to a funnel leading to the α -helical native state. Three smaller metastable funnels are also present, corresponding to three types of three-stranded β -sheets that differ in the length of the strands. Despite the significant time spent in a variety of unfolded configurations, the extended chain does not appear explicitly in Fig. 1(a) because the RMSD clustering scheme splits this state into many sequentially connected groups of unstructured con-

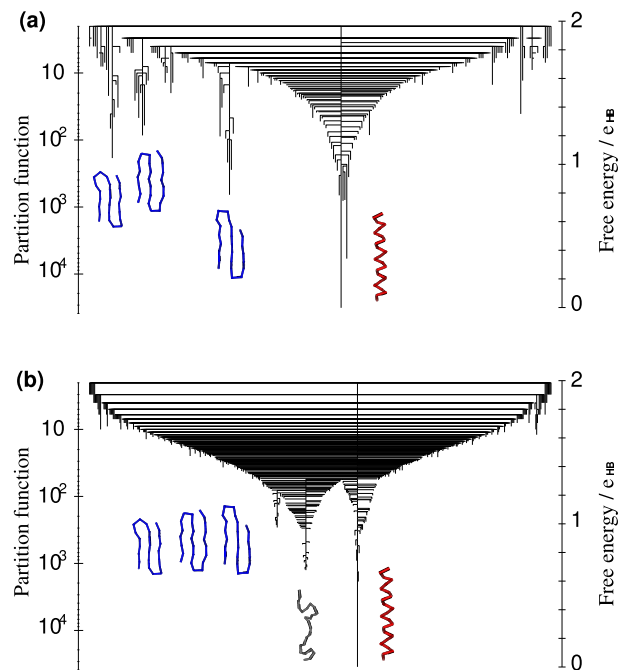


FIG. 1: TRDGs for tube parameters $e_S = 0.4$ and $e_W = 0.05$ at temperature $T^* = 0.161$. Configurations are grouped (a) by RMSD, and (b) by the order parameters (h, l, n) .

figurations, in contrast to the structurally well-defined folded states.

As noted above, the construction of TRDGs relies on the availability of an ergodic dynamical trajectory that samples all the configurations of interest. However, equilibrium trajectories of computationally feasible lengths do not sample metastable states correctly on a complex landscape, where large free energy barriers must be surmounted to reach them. To mitigate these problems, biased sampling techniques can be employed, accepting that the resulting trajectories cannot be interpreted dynamically. It is convenient in such simulations to project the configuration space on to a set of order parameters; we have chosen h , the number of hydrophobic contacts, and l and n , the number of local and non-local hydrogen bonds, respectively. The triplet (h, l, n) can discern the common structural motifs adopted by the tube. To test the effect of the projection, we apply it to the dynamic trajectory depicted in Fig. 1(a) to draw a companion TRDG (Fig. 1(b)) where states are defined by the values of h , l and n , rather than by RMSD clustering. The most prominent feature in Fig. 1(b) is again the funnel of the α -helix, but now the three metastable β -sheet states appear as one feature, since the order parameters do not distinguish between them. The projected graph clearly shows the metastable free energy minimum of the extended chain, which corresponds to a large volume of configuration space where (h, l, n) are all close to zero.

Although some differences arise from the choice of the clustering method, the two TRDGs in Fig. 1 present a consistent picture of the FEL. For example, the total relative partition function (obtained by summing the contri-

butions of individual branches) of the three β -sheet structures in Fig. 1(a) is 2179, while the corresponding funnel in Fig. 1(b) sums to a comparable 2565. The height of free energy barriers is also somewhat affected by the projection, but the organization of the graph according to structural motifs is not. The (h, l, n) projection will be used in the biased simulations that follow.

To sample the FEL extensively under conditions where large barriers exist, we implemented umbrella sampling [23] using a parabolic potential in l and n . The minimum of the umbrella potential was placed in turn over points on a grid in these two order parameters to generate a series of overlapping sampling windows. Each run was further enhanced by parallel tempering with four or six stages of temperature covering a range over which all states from native to fully unfolded are explored. The probability histograms $P(h, l, n)$ from all the runs were combined using the multiple histogram technique [24], enabling the free energy $F(h, l, n) = F_{\text{ref}} - kT \ln P(h, l, n)$ to be determined for a wide range of the order parameters up to the arbitrary constant F_{ref} .

Since $F(h, l, n)$ is a function of three variables, it cannot be depicted by a contour plot. We therefore adopted a graphical representation that shows the organization of basins (thermodynamically stable regions) and saddles (free energy barriers) of $F(h, l, n)$. A basin is represented by its lowest point, a local minimum of $F(h, l, n)$ defined by a triplet (h, l, n) for which a unit change in any individual order parameter or combination of order parameters leads to a higher free energy. A saddle point between two basins is the triplet of lowest free energy from which both basins can be reached by sequences of downhill stepwise changes in the order parameters. In this way, a network of nodes (basins) and edges (connecting saddles) is built up. A landscape topology graph (LTG) was then constructed analogously to a potential energy disconnectivity graph [25], by placing the nodes on a vertical free energy axis, and connecting pairs of nodes at the free energy of the highest saddle on the lowest contiguous path on $F(h, l, n)$ that joins them. Since each basin is represented only by its lowest point, the positions of the nodes and the vertical height of the branches in a LTG cannot be quantitatively identified with the total free energy of structures and barriers in the same way as in a TRDG. However, LTGs reveal particularly clearly the major features and organization of the FEL and will be seen in what follows to be consistent with TRDGs.

Fig. 2 shows LTGs for the 24-residue tube model under a variety of conditions. The top-left panel is dominated by a deep free energy minimum of an α -helical state. The only prominent metastable structure under these conditions is the β -sheet, with a β -hairpin and the extended chain only weakly metastable. The central and right-hand panels of Fig. 2 represent situations in which the hydrophobicity is increased with all other parameters held fixed. The α -helix and β -sheet are both destabilized with respect to various $\alpha\beta$ combinations and ultimately the β -barrel. By this stage the α -helix, though present,

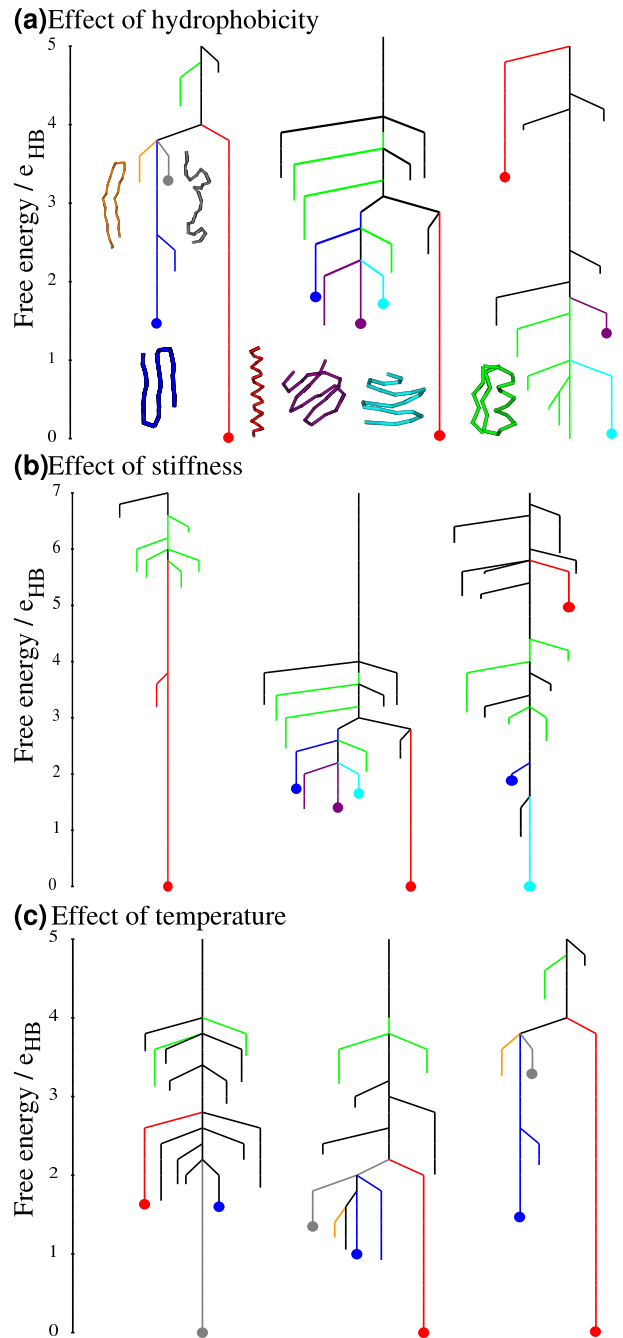


FIG. 2: LTGs illustrating the effect of: (a) hydrophobicity (with $e_s = 0.04$, $T^* = 0.141$ and $e_w = 0.04, -0.1, -0.2$), (b) chain stiffness (with $e_w = -0.1$, $T^* = 0.141$ and $e_s = 0.2, 0.4, 0.6$) and (c) temperature (with $e_s = 0.4$, $e_w = 0.05$ and $T^* = 0.181, 0.16, 0.141$). The branches that correspond to the structural motifs depicted in panel (a) are color-coded accordingly.

lies at such high free energy that it is unlikely to play a role in equilibrium folding.

Fig. 2(b) shows the effect of increasing stiffness at constant hydrophobicity. In all cases, the α -helix, β -sheet and β -helix are present. Altering the stiffness primarily adjusts the balance of stability between the α -helix and the various β -strand motifs, while some $\alpha\beta$ combinations are metastable on each FEL. Overall, therefore, the α -

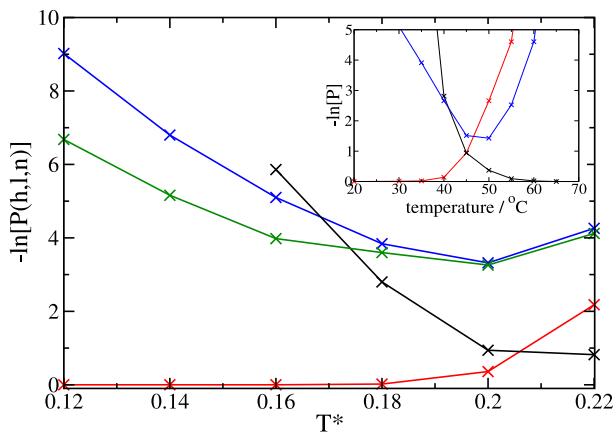


FIG. 3: Free energies (structure color code as for Fig. 2) as a function of reduced temperature for $\epsilon_S = 0.2$ and $\epsilon_W = 0.05$. Inset: comparison with the native (red line), unfolded (black) and intermediate (blue) states of human lysozyme, where P is the experimentally determined population from Ref. [26].

helix is favored by low stiffness and hydrophobicity, while competition arises with β -strands at higher stiffness, and with more compact structures at higher hydrophobicity. Thus, metastable states are generally present but are small in number as a result of the energetic and steric restrictions on the configuration space.

An increase in the number of residues in the polypeptide chain produces only a modest increment in the complexity of the FEL. We found that chains of 24, 36 and 48 residues at $T^* = 0.12$, $\epsilon_W = 0.05$ and $\epsilon_S = 0.4$ exhibit LTGs (not shown) with 5, 18 and 38 minima, respectively. Importantly, the number of prominent features (long branches) on the graphs remains small, increasing only from 2 to 4.

If the tube parameters are held fixed while the temperature is varied, we see in Fig. 2(c) that the balance between the free energies of the α -helix and β -sheet is subtly altered, but, as expected, the main effect of increasing the temperature is to stabilize the extended chain with respect to all compact structures. The LTG in the central panel is drawn at the folding temperature, where folded and unfolded structures compete equally.

The temperature-dependent competition is further examined in Fig. 3 in terms of $-\ln P(h,l,n)$ (i.e., free energy in units of the associated thermal energy), for the (h,l,n) of lowest free energy in each structural type. As already seen in Fig. 2(c), the native α -helix is gradually destabilized with respect to the extended chain with increasing temperature. However, the stabilities of the β -sheet and $\alpha\beta$ combinations change nonmonotonically. Starting from low temperatures, their thermal populations first rise, but, like those of all compact structures, then fall because of the high entropy of the extended chain. Non-native states thus exhibit maximum stability close to the folding temperature while always remaining metastable. The experimentally-determined temperature dependence of the stability of an amyloidogenic intermediate state of lysozyme (inset of Fig. 3) [26] closely

resembles the competition between stable, metastable and extended states shown in Fig. 3, thus linking our results to the misfolding process of proteins, which is often accompanied by pathogenic aggregation [26, 27].

The conceptual picture that emerges from the present work is that the characteristic FEL of a polypeptide chain is dominated by a particular family of related structures, and that additionally contains a small number of metastable states. Our results also indicate that there are specific conditions under which these metastable states are likely to play a major role in determining the balance between folding and misfolding.

-
- [1] K. A. Dill and H. S. Chan, *Nat. Struct. Biol.* **4**, 10 (1997).
 - [2] A. R. Dinner, A. Šali, L. J. Smith, C. M. Dobson, and M. Karplus, *Trends Biochem. Sci.* **25**, 331 (2000).
 - [3] J.-E. Shea and C. L. Brooks 3rd., *Annu. Rev. Phys. Chem.* **52**, 499 (2001).
 - [4] J. N. Onuchic and P. G. Wolynes, *Curr. Opin. Struct. Biol.* **14**, 70 (2004).
 - [5] S. E. Radford, C. M. Dobson, and P. A. Evans, *Nature* **358**, 302 (1992).
 - [6] J. Rumbley, L. Hoang, L. Mayne, and S. W. Englander, *Proc. Natl. Acad. Sci. USA* **98**, 105 (2001).
 - [7] F. Khan, J. I. Chuang, S. Gianni, and A. R. Fersht, *J. Mol. Biol.* **333**, 169 (2004).
 - [8] D. M. Korzhnev *et al.*, *Nature* **430**, 586 (2004).
 - [9] U. Mayor *et al.*, *Nature* **421**, 863 (2003).
 - [10] J. Gsponer *et al.*, *Proc. Natl. Acad. Sci. USA* **103**, 99 (2006).
 - [11] P. J. Booth, *Fold. & Des.* **2**, 85 (1997).
 - [12] V. McParland, A. Kalverda, S. Homans, and S. Radford, *Nat. Struct. Biol.* **9**, 326 (2002).
 - [13] C. M. Dobson, A. Šali, and M. Karplus, *Angew. Chem. Int. Ed.* **37**, 868 (1998).
 - [14] S. V. Krivov and M. Karplus, *Proc. Natl. Acad. Sci. USA* **101**, 14766 (2004).
 - [15] S. V. Krivov and M. Karplus, *J. Chem. Phys.* **117**, 10894 (2002).
 - [16] J. M. Carr and D. J. Wales, *J. Chem. Phys.* **123**, 234901 (2005).
 - [17] A. Šali, E. I. Shakhnovich, and M. Karplus, *Nature* **369**, 248 (1994).
 - [18] T. X. Hoang, A. Trovato, F. Seno, J. R. Banavar, and A. Maritan, *Proc. Natl. Acad. Sci. USA* **101**, 7960 (2004).
 - [19] J. R. Banavar *et al.*, *Phys. Rev. E* **73**, 031921 (2006).
 - [20] S. Auer, C. M. Dobson, M. Vendruscolo, *HFSP J.* **1**, 137 (2007).
 - [21] H. M. Berman *et al.*, *Nucleic Acids Res.* **28**, 235 (2000).
 - [22] Y. Zhang, I. A. Hubner, A. K. Arakaki, E. Shakhnovich, and J. Skolnick, *Proc. Natl. Acad. Sci. USA* **103**, 2605 (2006).
 - [23] G. M. Torrie and J. P. Valleau, *Chem. Phys. Lett.* **28**, 578 (1974).
 - [24] A. M. Ferrenberg and R. H. Swendsen, *Phys. Rev. Lett.* **63**, 1195 (1989).
 - [25] O. M. Becker and M. Karplus, *J. Chem. Phys.* **106**, 1495 (1997).
 - [26] P. Haezebrouck *et al.*, *J. Mol. Biol.* **246**, 382 (1995).
 - [27] D. R. Booth *et al.*, *Nature* **385**, 787 (1997).